# Towards Controlling the Solid State Valence Tautomer Interconversion Character by Solvation

Marcos A. Ribeiro[1], Daniel E. Stasiw[2], Philip Pattison[3], Paul R. Raithby[4], David A. Shultz[2] and Carlos B. Pinheiro[1*].

1- Departamento de Física, Universidade Federal de Minas Gerais, Belo Horizonte, Brazil.

2- Department of Chemistry, North Carolina State University, Raleigh, USA,

3- Swiss-Norwegian Beam Line, ESRF, Grenoble Cedex, France

4- Department of Chemistry, University of Bath, Bath, BA2 7AY, United Kingdom.

*E-mail: cbpinheiro@ufmg.br

*KEYWORDS Valence Tautomers, cobalt, dioxolene.*

**ABSTRACT:** Crystals of [Co*(diox)*$_2$(4-NO$_2$-py)$_2$] (***1***) and [Co*(diox)*$_2$(4-CN-py)$_2$](***2***) where *diox* are the *o*-Dioxolene 3,5-di-*t*-butylsemiquinonate ($SQ^{\bullet-}$)and/or 3,5-di-*t*-butylcatecholate ($Cat^{2-}$)ions, 4-NO$_2$-py is 4-nitro-pyridine, 4-CN-py is 4-cyano-pyridine, are among the few known crystals presenting both thermal-induced and photoinduced *ls*-[$M^{+3}(SQ^{\bullet-})(Cat^{2-})$] ↔*hs*-[$M^{2+}(SQ^{\bullet-})_2$]valence tautomerism interconversion (VTI). In ***2*** the thermal-induced VTI is cooperative, characterizing an abrupt conversion and in ***1*** it is non-cooperative. In this work, crystals of [Co*(diox)*$_2$(4-NO$_2$-py)$_2$]·benzene (***1BZ***), [Co*(diox)*$_2$(4-NO$_2$-py)$_2$]·toluene (***1TL***), [Co*(diox)*$_2$(4-CN-py)$_2$]·benzene (***2BZ***) and [Co*(diox)*$_2$(4-CN-py)$_2$]·toluene (***2TL***) have been prepared and analyzed by single crystal X-ray diffraction in order to investigate how solvation modulates thermal-induced VTI. The solvate crystals, like the non-solvated ones, present essentially reversible thermal-induced and photoinduced VTI. ***1TL*** crystal presents the same monoclinic symmetry and the same intermolecular hydrogen-bonded network of ***1*** and both present a non-cooperative thermal-induced VTI. ***1BZ*** crystal has triclinic symmetry and present a cooperative and abrupt VTI with a thermal hysteresis of ~30 K. In contrast to ***2***, thermal-induced VTI in ***2BZ*** and ***2TL*** is non-cooperative despite the fact that ***2***, ***2BZ*** and ***2TL*** crystals exhibit the same monoclinic symmetry and the same intermolecular hydrogen-bonded network. In ***2BZ*** and ***2TL***benzene and toluene molecules as well as the *t*-butyl groups of the *o*-dioxolene molecules convert gradually from being dynamically disordered at about 300 K to a static disorder state below 150 K. The layer separation distance of interacting [Co*(diox)*$_2$(4-X-py)$_2$], X=CN and NO$_2$, molecules in all solvate crystals is ~15 Å whereas in the ***2,*** which presents cooperative VTI, it is ~12 Å. An order-disorder component might account to the stabilization of the metastable *hs*-$Co^{2+}$ state in ***2BZ*** and in ***2TL*** but no disorder was found in the ***1TL*** crystals. Therefore, the lack of cooperativeness in the thermal-induced VTI in these crystals seems to be due to the large distance between the layers of interacting molecules. Cooperativeness in the VTI of ***1BZ*** crystal is likely to be related with the unique molecular bond scheme network that connects neighboring active [Co*(diox)*$_2$(4-NO$_2$-py)$_2$] molecules through the *o*-Dioxolene oxygen atoms bonded directly to the *Co* ion.

## Introduction

Functional molecular materials possess at least two distinct states that interconvert when subject to an external stimuli. Their proprieties can be enhanced and/or adjusted through chemical changes and thus it is important to understand the forces driving their formation and organization as well as the mechanisms of interaction between individual active units. The study of functional molecular materials can therefore help in the development of molecular scale electronic devices.[12]Valence tautomers[3] are electronically labile compounds showing charge transfer between redox active ligands and a metallic center followed by the change of electronic spin of the metal. The electronic states in the valence tautomers are nearly degenerate and this leads to vibronically coupled interactions with an appreciable sensitivity to the environment.[4]The valence tautomerism interconversion (VTI) is essentially entropically driven,[5] associated with remarkable variations in the optical and magnetic properties and can be modulated with chemical changes. VTI is induced by external stimuli such as irradiation by light[6,7] soft[8] and hard X-rays[,9] and by changes such as temperature or pressure. [10,11.]VTI can be described by the following reaction scheme:

$$ls\text{-}[M^{(n+1)}L^{(m+1)}] \leftrightarrow hs\text{-}[M^{n}L^{m}]$$

where *ls* stands for the low spin state, *hs* for the high spin state, *M* for the metal ion and *L* for redox ligands., and in a formal sense, this equation is similar to the one used to describe the spin-crossover[12] equilibrium. The VTI involves a change of the electronic population of the anti-bonding $e_g^*$ metal orbitals that affects the length of the metal-ligand bond and the exothermic/endothermic character of the interconversion. At low temperatures, where the free energy changes are largely determined by the enthalpy contributions, the tautomer ground state is characterized by unpopulated anti-bonding $e_g^*$ orbitals and thus by short metal-ligand bonds. However, re-

versible metastable states at very low temperatures can also be induced by light irradiation[13],[14]. The lifetime of this photoinduced metastable species depend on the free energy barrier of the relaxation process and decay seems to begin as soon as the light stimulus is removed [15,16]. Typical examples of valence tautomers are coordination compounds of cobalt, and *o*-dioxolene ligands and ancillary amine ligands.[5,17] In these complexes the *o*-dioxolene organic moiety binds the metal ion in two different redox states: as a bi-negative catecholate ($Cat^{2-}$) and a mono-negative radicalar semiquinonate ($SQ^{\bullet-}$). The *o*-dioxolene ligands can have filled or partially filled molecular orbitals that are close in energy to the *Co d*-orbitals allowing moderated interactions with the metal *d*-orbitals, even though the metallic and free ligand orbitals characters are kept. The extension of this interaction is enough to keep the separation of the metal and ligand orbitals in the order to allow electron transfer between them, followed by changing in the metal multiplicity. Since the frontier orbitals have preferentially metal and ligand based character it is possible to change the charge distribution in the complexes by changing the redox potential of the *o*-dioxolene derivative ligand and the nature of ancillary ligands. Adams *et al*[18] reported the first observation of VTI in solid state for the compound of [Co*(diox)*$_2$(*phen*)], where diox are the 3,5-di-*t*-butylsemiquinonate and/or 3,5-di-*t*-butylcatecholate ions and *phen* is phenanthroline. In this seminal work, the interconversion characteristics were investigated by correlating the single crystal X-ray structural data at room and low temperatures with the temperature-dependent magnetic moment ($\mu_{eff}$) measurements for non-solvate, toluene, methyl cyclohexane and chorobenzene solvates as well as for toluene desolvated samples. The critical role played by the ordering-disordering process of the solvate toluene molecules in determining the cooperative and abrupt character of the VTI was established. Crystals of [Co*(diox)*$_2$(4-$NO_2$-py)$_2$] (***1***), [Co*(diox)*$_2$(4-CN-py)$_2$] (***2***) and [Co*(diox)*$_2$(4-Br-py)$_2$] (***3***), were first studied with respect to the thermo and photoinduced VTI (scheme I).[19,20] Additionally, Schmidt *et al* have also noted the influence of solvent in the crystal packing and its role in the interconversion, showing a more gradual interconversion for toluene solvated crystal.[19]

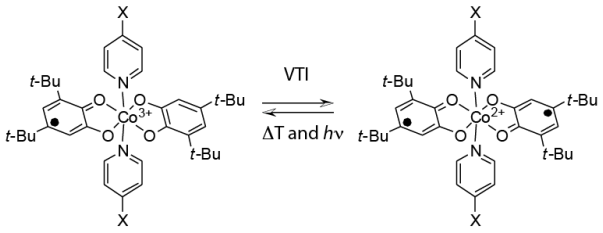


**Scheme I: VTI *ls*-[$Co^{+3}(SQ^{\bullet-})(Cat^{2-})$]↔*hs*-[$Co^{2+}(SQ^{\bullet-})_2$] in [Co*(diox)*$_2$(4-X-py)$_2$] complexes; X=CN, $NO_2$ and Br**

It was reported that VTI in ***1*** is non-cooperative and takes place over a large temperature range exhibiting pure *ls*-[$Co^{+3}(SQ^{\bullet})(Cat^{2-})$] state below 110 K whereas in ***2*** and in ***3*** VTI is cooperative and abrupt, exhibiting pure *ls*-[$Co^{+3}(SQ^{\bullet-})(Cat^{2-})$] state below 150 K and 100 K, respectively. In this work crystals of [Co*(diox)*$_2$(4-$NO_2$-py)$_2$]·benzene (***1BZ***), [Co*(diox)*$_2$(4-$NO_2$-py)$_2$]·toluene (***1TL***), [Co*(diox)*$_2$(4-CN-py)$_2$]·benzene and (***2BZ***), [Co*(diox)*$_2$(4-CN-py)$_2$]·toluene (***2TL***), (scheme II), have been prepared and analyzed by temperature dependent single crystal X-ray diffraction in order to investigate how solvation modulates thermal-induced VTI properties.

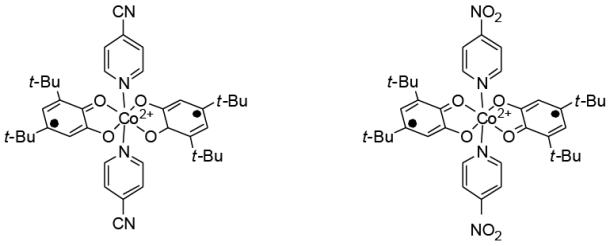


**Scheme II: [Co*(diox)*$_2$(4-CN-py)$_2$] and [Co*(diox)*$_2$(4-$NO_2$-py)$_2$] complexes**

## Experimental

### Complexes synthesis and characterization

All of the chemicals for syntheses and analysis were of analytical grade and used without further purification. The preparation of [Co*(diox)*$_2$(4-$NO_2$-py)$_2$] and [Co*(diox)*$_2$(4-CN-py)$_2$] have been previously reported[19]. Solvated single crystals samples suitable for X-ray diffraction were grown by slow evaporation in test tube over $N_{2(g)}$ atmosphere and kept in this condition until the measurements.

### Instrumental details

X-ray diffraction data collections were performed using Oxford-Diffraction *GEMINI* diffractometers at home facilities and at the Swiss Norwegian Beam Line, ESRF-France. Measurements were performed during heating and cooling processes with temperatures ranging from 290 K down to 90 K. An Oxford Cryojet device with precision better than ±2 K was used to control the samples temperatures during the experiments. For data consistency, temperature dependent measurements were always performed using the same sample. Table S1 in the supplementary information (SI) shows the details of the different measurements performed.

### Structure determination by single crystal X-ray diffraction

For all samples investigated, the X-ray diffraction data integration and scaling of reflections intensities were performed with the *Crysalis suite*.[21] Final unit cell parameters were based on the fitting of all measured reflections positions. Analytical[22] and Semi-Empirical[23] absorption corrections were performed using *Crysalis suite*.[21]The program *XPREP*[24] was used for the space group identification and final data reduction. The structures of all compounds were solved by direct methods using the *SIR92*[25] program. For each compound, the positions of all but the hydrogen atoms could be unambiguously assigned on consecutive difference Fourier maps. Refinements were performed using *SHELXL*2013[26] based on $F^2$ through full-matrix least square routine. During the refinements disordered *t*-butyl groups and solvate molecules were identified and modeled with split atomic positions. All, except the hydrogen atoms, were refined with anisotropic atomic displacement parameters. The hydrogen atoms in the compounds were added in the

structure in idealized positions and further refined according to the riding model.[27] $U_{iso}$(H) = 1.2$U_{eq}$(C) for aromatic molecules and $U_{iso}$(H) = 1.5$U_{eq}$(C) for methyl groups. CCDC 1448193, , 1448194, 1448195, 1448196, 1448197, 1448198, 1448310 and 1448311 contains the supplementary crystallographic data for this paper. The data can be obtained free of charge from The Cambridge Crystallographic Data Centre via www.ccdc.cam.ac.uk/getstructures.

## Structure description

The single crystal X-ray diffraction data were used to investigate the structural properties of ***1BZ***, ***1TL***, ***2BZ*** and ***2TL*** including the geometry of pure *ls*-[$Co^{+3}(SQ^{\bullet-})(Cat^{2-})$] and *hs*-[$Co^{+2}(SQ^{\bullet-})_2$] states, the solvates position and orientation as well as to follow the changes in the crystalline structure upon heating and cooling. The *hs*-[$Co^{+2}(SQ^{\bullet-})_2$]↔*ls*-[$Co^{+3}(SQ^{\bullet-})(Cat^{2-})$] interconversion can be investigated by temperature dependent single crystal X-ray diffraction techniques, since this technique provides very accurate bond-distance measurement with precision much smaller than the distances changes caused by VTI. Usually $Co^{2+}$–*L* bond lengths are 0.1 to 0.2 Å longer than those observed for $Co^{3+}$–*L* (*L* = ligand atom nearby the metal ion). The *C–O* and *C–C* bond distances of the redox-active ligands also change according to the $SQ^{\bullet-}$ or $Cat^{2-}$ oxidation state of the ligands. *C–O* bond lengths are longer than 1.34 Å in the $Cat^{2-}$ whereas the *C=O* bond lengths in the $SQ^{\bullet-}$ are ~1.30 Å. *C–C* bond lengths in $Cat^{2-}$ are slightly longer (~0.2 Å) than the ones found in $SQ^{\bullet-}$ due to the higher aromaticity of $Cat^{2-}$. Finally the *C–C* bond length of the aromatic carbon atoms bonded to the two oxygen atoms binding the *Co* ion is shorter in the $Cat^{2-}$ than in $SQ^{\bullet-}$. ***1BZ***, ***1TL***, ***2BZ*** and ***2TL*** sample characteristics, data collection and refinements parameters for representative temperature measurements are indicated in SI Tables S2 and S3.

In the structures of ***1BZ***, ***1TL***, ***2BZ*** and ***2TL*** solvate crystals, the *Co* atoms sit on a inversion center, hence only half of each [Co*(diox)*$_2$(4-$NO_2$-py)$_2$] and [Co*(diox)*$_2$(4-CN-py)$_2$] molecules are crystallographically independent. Since the *Co* ions in these complexes have an octahedral coordination there are only two *Co–O* (namely *Co-O1, Co-O2*) and one *Co-N* independent refined distances in the structures. Consequently, the mixed valence $Cat^{2-}/SQ^{\bullet-}$ delocalization around the *Co* atoms in the *ls*-[$Co^{+3}(SQ^{\bullet-})(Cat^{2-})$] state cannot be investigated by the analysis of the interatomic distances obtained from the X-ray diffraction data. Figure 1 shows the molecular structure and the atomic labeling scheme for the atoms in the asymmetric unit of ***1BZ***, ***1TL***, ***2BZ*** and ***2TL*** crystals. In all crystals, pyridine rings coordinate the *Co* ion in a *trans* conformation, with the orientation of the pyridine ring defined by the steric hindrance of *t*-butyl group in the position of the C6 atom and by four intramolecular $C_{ar}$–$H^{\cdots}O_{diox}$ hydrogen bonds between the adjacent carbon atoms of the pyridine and one oxygen atom of the dioxolene moiety as listed in SI Tables S4-7. Benzene and toluene solvate molecules are also bonded to the structures through hydrogen bonds between carbon solvent atoms and terminal nitro and cyano groups. π-stacking interactions between pyridine and solvent aromatic rings may to contribute to keeping these groups parallel.

### Co*(diox)*$_2$(4-$NO_2$-py)$_2$

Non-solvated [Co*(diox)*$_2$(4-$NO_2$-py)$_2$] (***1***) and ***1TL*** crystal structures are similar and described by the monoclinic $P2_1/c$

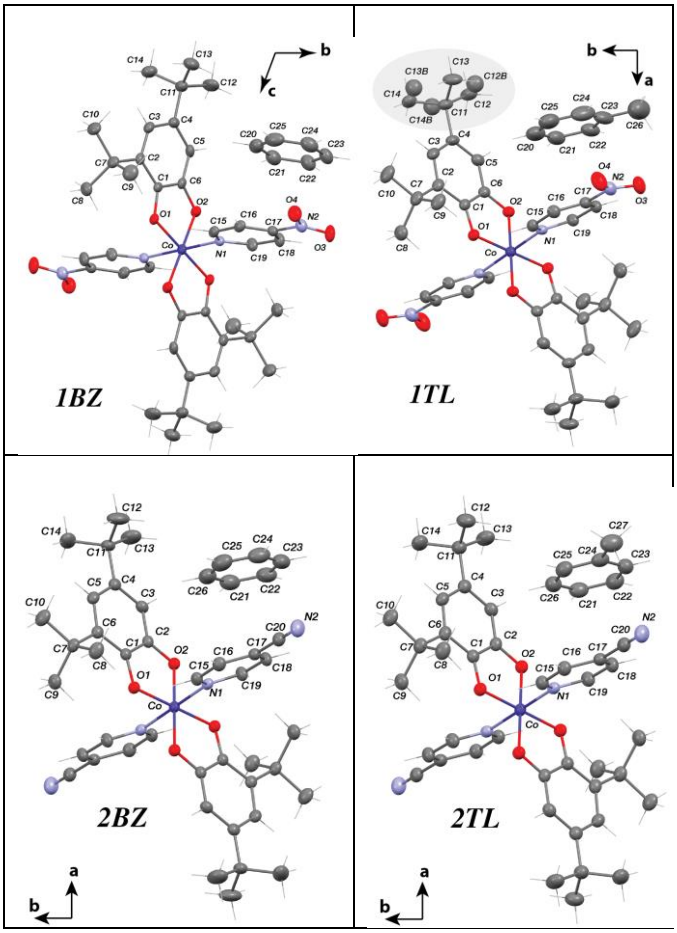


Figure 1. Molecular geometry and atomic labeling scheme used in the description of ***1BZ*** (110 K), ***1TL*** (100 K), ***2BZ*** (123 K) and ***2TL*** (123 K) structures. Only atoms of the asymmetric units are labeled. Ellipsoids are drawn at 50% of probability levels. Hydrogen atoms are represented in wireframe style for the sake of clarity. The grey circle in the ***1TL*** structure highlights the disordered *t*-butyl groups.

space group symmetry, with four molecules in the asymmetric unit (Z=2). The *t*-butyl groups in ***1TL*** crystal were found to be disordered over the full temperature range investigated and were modeled with atomic split positions. The structure of the ***1BZ*** crystal is described by the triclinic $P\bar{1}$ space group symmetry with Z=1. The ***1BZ*** crystal structure is ordered over the whole temperature range investigated. Both ***1BZ*** and ***1TL*** solvate crystals do not show any change in their crystallographic symmetry upon cooling.

The X-ray diffraction data analysis shows that thermal-induced VTI in both ***1BZ*** and ***1TL*** crystals are followed by major structural reversible changes. ***1TL*** crystals contract in all directions whereas the ***1BZ*** expands in the ***a*** direction and contracts in the ***b*** and ***c*** directions while the overall unit cell volume is also reduced upon cooling (Figure 2a,b). It was observed during the *hs*-[$Co^{+2}(SQ^{\bullet-})_2$]→*ls*-[$Co^{+3}(SQ^{\bullet-})(Cat^{2-})$]

conversion of both solvates that an isotropic contraction of the *Co–L* distances of approximately 0.15 Å occurred. The *Co–L* distances during the cooling change abruptly for ***1BZ*** at ~120 K and smoothly for ***1TL*** over the entire investigated temperature range (Figure 2c,d). The *Co–L* distances contraction/expansion upon cooling and heating reveal a remarkable hysteresis of~30 K for ***1BZ*** (Figure 2c). Following the overall unit cell and *Co–L* distance changes upon cooling and heating process, the solvents molecules, $NO_2$ and pyridine moieties also change their relative orientation in both the ***1BZ*** and ***1TL*** complexes. In ***1BZ*** solvate benzene molecules interact with $NO_2$ group keeping their relative orientation unchanged upon cooling and heating. However both the $NO_2$ group and the solvate benzene molecules change their relative orientation abruptly and reversibly in relation to the pyridine ring plane during the VTI (Figure 2e). In ***1TL*** only smooth changes in the orientations of the the $NO_2$, pyridine and toluene ring planes are observed (Figure 2,f).

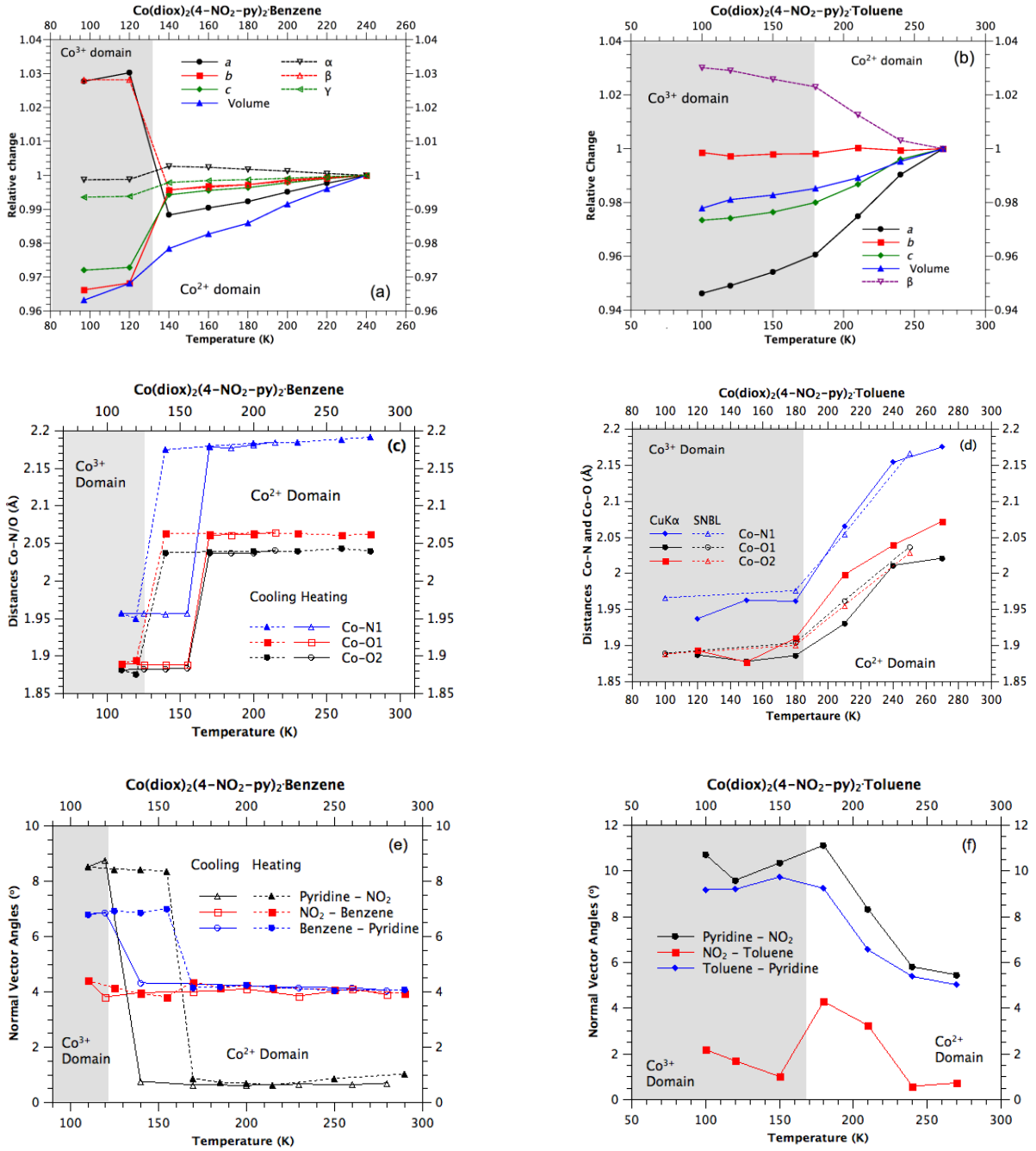


Figure 2. Relative changes in the lattice parameters of (a) ***1BZ*** and (b) ***1TL*** crystals upon cooling. Behavior of the interatomic *Co–O* and *Co–N* distances in ***1BZ*** (c) and in ***1TL*** (d) computed from the analysis of the temperature dependent X-ray diffraction data. *Co-L* distance for ***1TL*** was computed after the refinement of a low-resolution data (CuKα) and high-resolution data obtained at the Swiss Norwegian Beam Line at the ESRF (SNBL).Angles between normal vector from solvents, $NO_2$ and pyridine ring planes in (e) ***1TL*** and (f) ***1BZ*** crystals upon cooling.

The superposition of the non-solvated crystal structure of ***1*** with those of the solvate forms ***1TL*** and ***1BZ*** are shown in Figure 3. The toluene solvate molecule in ***1T L***and the benzene solvate in ***1BZ*** structures increase the separation between the layers of [Co*(diox)*$_2$(4-NO$_2$-py)$_2$] interacting molecules by *ca.* 20% when compared with the non-solvated form ***1***. This is reputed to contribute to the weakening of the *t*-butyl interactions and to the lack of cooperativety in the VTI in ***1***[19,20].

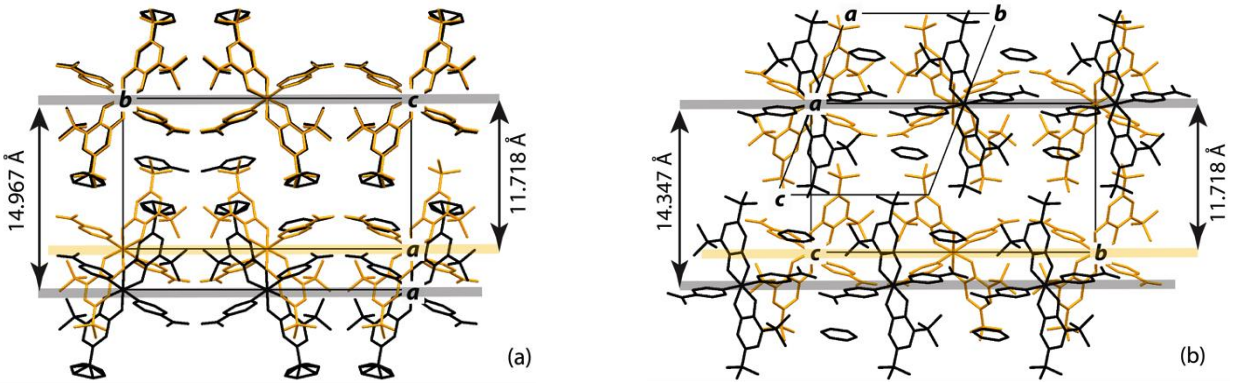


Figure 3: (a) Superposition of the structures of the non-solvated [Co*(diox)*$_2$(4-NO$_2$-py)$_2$] (orange) and ***1TL*** (black). (b) (a) Superposition of the structures of the non-solvated [Co*(diox)*$_2$(4-NO$_2$-py)$_2$] (orange) and ***1BZ***(black). Both, toluene and benzene solvation molecules increase the separation between the layers of interacting [Co*(diox)*$_2$(4-NO$_2$-py)$_2$] molecules. Unit cell directions are indicated. Hydrogen atoms were omitted for sake of clarity.

In ***1***, ***1BZ*** and in ***1TL*** structures, [Co*(diox)*$_2$(4-NO$_2$-py)$_2$] in layer molecules are linked by two major hydrogen bonds types: $C_{ar}$–$H^{\cdots}O_{diox}$ and $C_{ar}$–$H^{\cdots}ONO$, where $C_{ar}$ are aromatic carbon atoms of the pyridine ring and $O_{diox}$ stands for an oxygen atoms of the dioxolene group binding the cobalt ion (Figure 4). Four $C_{ar}$–$H^{\cdots}O_{diox}$ bonds are observed between [Co*(diox)*$_2$(4-NO$_2$-py)$_2$] neighbor moieties in both ***1BZ*** and ***1TL*** crystals: the oxygen atom O2 of the dioxolene acts as acceptor in two while the carbon atom C16 of pyridine ring acts as a donor in other two H-bonds (Figure 4b,d). As evidenced by the distances shown in Table 1, the shortest and therefore the strongest $C_{ar}$–$H^{\cdots}O_{diox}$ bonds between neighbors molecules were found for ***1BZ*** crystals. Thus, solvation seems to affect only the strength but not the number of these *H*-bonds. $C_{ar}$–$H^{\cdots}ONO$ interactions also control the packing of the ***1***, ***1BZ*** and in ***1TL*** structures and solvation does affects the number, but not the strength, of such bonds between neighboring molecules as indicated in Table 1. For the ***1BZ*** solvate crystal four $C_{ar}$–$H^{\cdots}ONO$ interactions are observed for each molecule whereas for ***1*** and for ***1TL*** solvate crystal only two of such interactions are observed, as indicated in Figure 4.

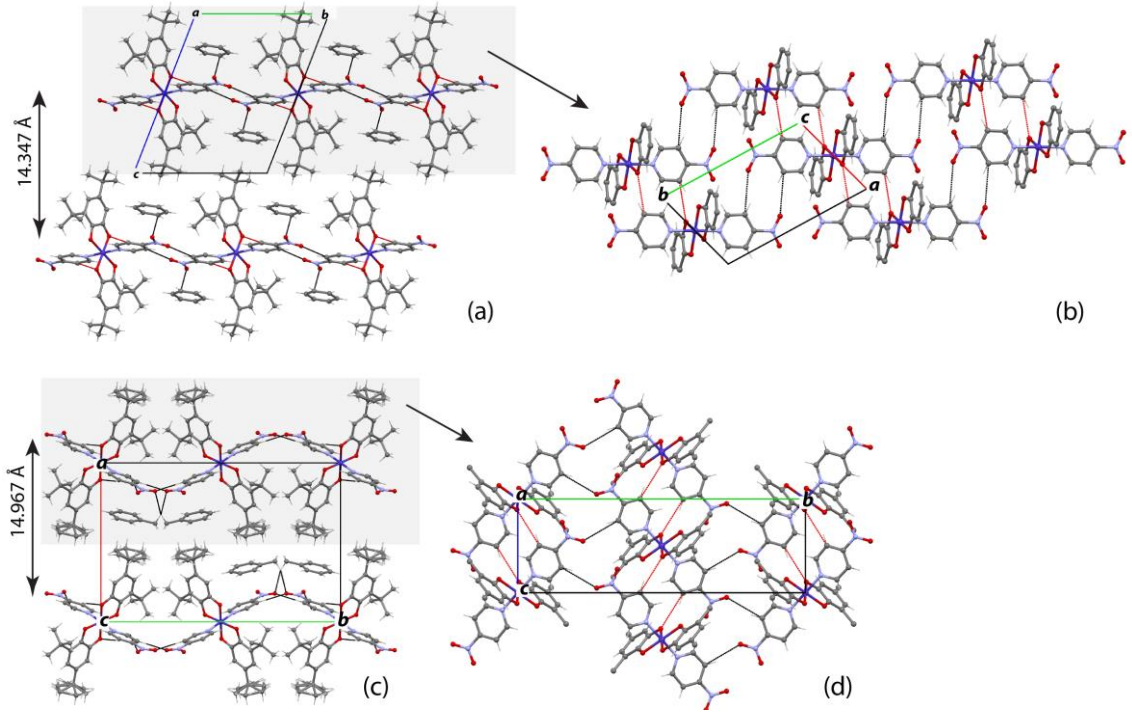

Figure 4: View of the crystal packing of the (a) ***1BZ*** and (c) ***1TL***solvate crystals towards ***c*** direction. Interaction between solvent molecules and $NO_2$ group are also indicated. In-layer (grey shadow)$C_{ar}$–$H$···$O_{diox}$ and $C_{ar}$–$H$···$ONO$ hydrogen bonds between neighbor molecules shown in (b) and (d) towards ***a*** direction are represented in red and black lines respectively. The *t*-butyl groups of the dioxolene moieties in (b) and (d) are omitted for clarity

## Co*(diox)*$_2$(4-CN-py)$_2$

Similarly the crystal structure of the non-solvate [Co*(diox)*$_2$(4-CN-py)$_2$] ***(2)*** the ***2TL*** and ***2BZ*** solvate crystal structures are described by the $P2_1/c$ symmetry with Z=2. The VTI *hs*-[$Co^{+2}(SQ^{\bullet-})_2$]→*ls*-[$Co^{+3}(SQ^{\bullet-})(Cat^{2-})$] in both ***2TL*** and ***2BZ*** crystals is followed by an smooth isotropic contraction of the first coordination sphere around the *Co* ions by approximately 0.15 Å, by the reorientation of the toluene and benzene solvents and by an anisotropic unit cell volume contraction with no change in their crystal symmetry (Figure 5). The ***2BZ*** crystal structure is ordered over the temperature range investigated, whereas in the ***2TL*** crystal structure the solvate molecules and *t*-butyl groups convert from being dynamic to static disordered below 183 K. The ordering of the toluene influences the behavior of the monoclinic $\beta$ angle as well as the toluene-pyridine ring normal vector angles as indicated in (Figure 5c,d). Thus, as in ***2***, ***2TL*** also seems to show an order-disorder component in its VTI.

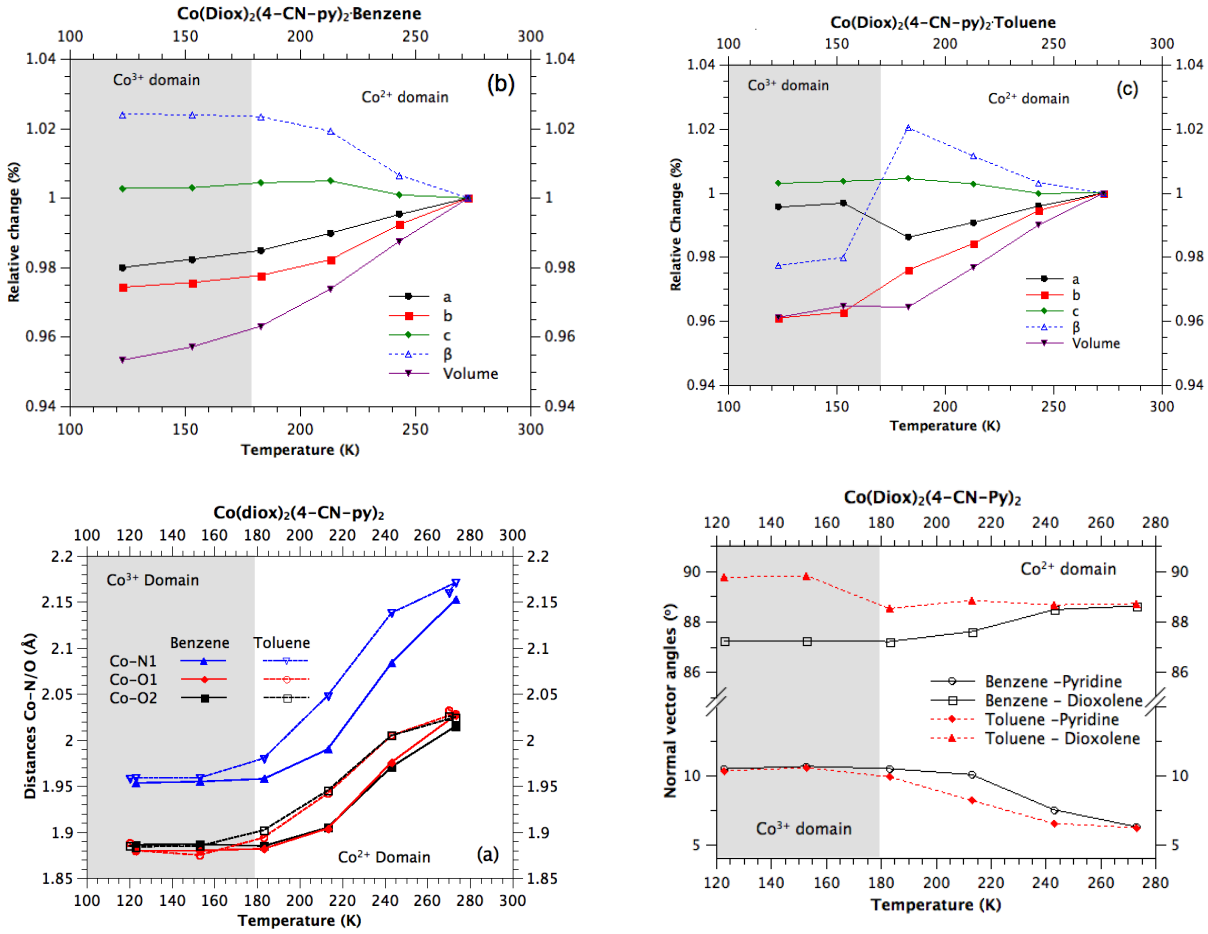


Figure 5: Relative changes in the lattice parameters of (a) ***2BZ*** and (b) ***2TL*** crystals upon cooling. (c) Behavior of the interatomic *Co–O* and *Co–N* distances in ***2BZ*** and in ***2TL*** computed from the analysis of the temperature dependent X-ray diffraction data. (d) Angles between normal vectors from solvents, dioxolene and pyridine molecule planes in ***2TL*** and***2BZ*** crystals upon cooling..

The superposition of ***2*** and the ***2BZ*** and ***2TL*** crystal structures are show in Figure 6. In the solvate crystals, the separation between the layers of [Co*(diox)*$_2$(4-CN-py)$_2$] interacting molecules increase by *ca.* 23% when compared with the non-solvated form. [Co*(diox)*$_2$(4-CN-py)$_2$] in layer molecules are linked by two major hydrogen bonds: $C_{ar}$–$H$···$O_{diox}$ and $C_{ar}$–$H$···$N_{cyano}$. The strength and geometrical properties of these bonds depend little on the solvent and on the temperature (Table 1).

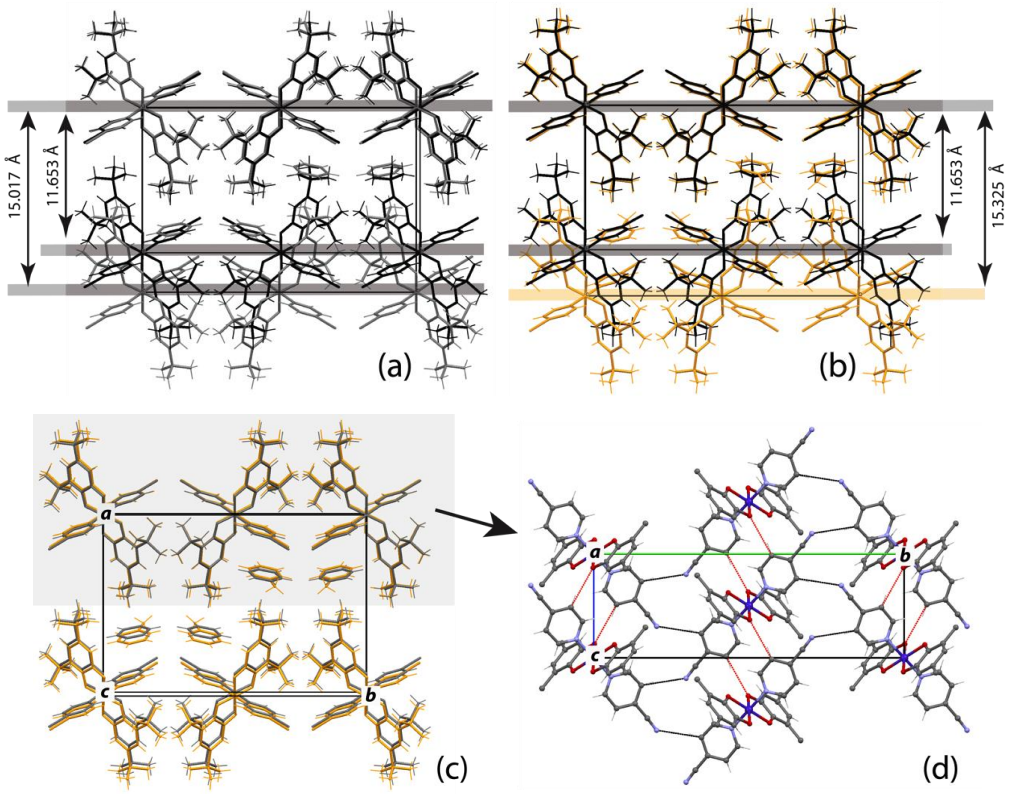


Figure 6: (a) Superposition of the structures of the non-solvated [Co*(diox)*$_2$(4-CN-py)$_2$] (grey) and ***2BZ*** (black) and (b) of [Co*(diox)*$_2$(4-CN-py)$_2$] (orange) and ***2TL*** (black). Both, toluene and benzene solvation molecules increase the separation between the layers of interacting [Co*(diox)*$_2$(4-CN-py)$_2$] molecules. The unit cell directions are indicated. (c) ***2BZ*** (black) and ***2TL*** (orange) superposition towards ***c*** direction. (d) In-layer $C_{ar}$–H···$O_{diox}$ and $C_{ar}$–H···$N_{cyano}$ interactions represented in red and black lines respectively towards ***a*** direction. *t*-butyl groups in (d) were omitted for clarity.

**Table 1: Selected distances in (Å) in *1*, *1TL*, *1BZ*, *2*, *2TL* and *2BZ*.**

| ***1BZ*** | 110 K | 280 K | ***1TL*** | 100 K | 250 K | ***1*** | 100 K | |
|---|---|---|---|---|---|---|---|---|
| C16-H16···O2$^{i}$ | 3.122(3) | 3.124(3) | C16-H16···O2$^{vi}$ | 3.319(3) | 3.337(3) | C16-H16...O2$^{xi}$ | 3.239(12) * | |
| C18-H18···O3$^{ii}$ | 3.293(3) | 3.323(3) | C18-H18···O3$^{ix}$ | 3.384(3) | 3.381(4) | C18-H18····O3 | 3.317(13)* | |
| C15-H15···O1 | 2.840(3) | 3.136(3) | C15-H15···O1 | 2.837 (3) | 3.051 (3) | C15-H15···O1 | 2.865(11)* | |
| C19-H19···O1$^{III}$ | 2.824(3) | 3.051(3) | C19-H19···O1$^{x}$ | 2.850 (3) | 3.084 (3) | C19-H19···O1$^{iv}$ | 2.844(12) * | |
| Co–Co$^{iv}$ | 6.9528(4) | 6.7872(3) | Co–Co$^{iv}$ | 7.3495(2) | 7.3742(2) | Co–Co$^{xi}$ | 7.2830(6) | |
| Co–Co$^{v}$ | 12.3420(8) | 12.7759(5) | Co–Co$^{v}$ | 11.7995(2) | 12.0695(2) | Co–Co$^{xii}$ | 11.7884(9) | |
| ***2BZ*** | 123 K | 273 K | ***2TL*** | 120 K | 270 K | ***2*** | 95 K | 143 K |
| C16-H16···O2$^{vi}$ | 3.228(3) | 3.238(4) | C16-H16···O2$^{xi}$ | 3.223(3) | 3.318(4) | C18-H18···O1$^{vi}$ | 3.209(6) | 3.185(4) |
| C18-H18···N2$^{vii}$ | 3.432(3) | 3.474(5) | C18-H18···N2$^{ix}$ | 3.425(3) | 3.508(5) | C16-H16···N2$^{xiii}$ | 3.391(6) | 3.389(6) |
| C15-H15···O1 | 2.821(2) | 3.023(4) | C15-H15···O1 | 2.819(3) | 3.046(4) | C15-H15···O2 | 2.840(6) | 3.047(5) |
| C19-H19···O1$^{viii}$ | 2.861(2) | 3.081(4) | C19-H19...O1$^{viii}$ | 2.866(3) | 3.088(4) | C19-H19···O1$^{xiv}$ | 3.138(5) | 3.507(4) |
| Co–Co$^{xi}$ | 7.316(5) | 7.2956(4) | Co–Co$^{iv}$ | 7.387(1) | 7.3621 (3) | Co–Co$^{xi}$ | 7.2851(5) | 7.211 |
| Co–Co$^{xii}$ | 11.637(3) | 11.9108(6) | Co–Co$^{xii}$ | 11.614(1) | 12.0095(4) | Co–Co$^{xii}$ | 11.7901(7) | 11.9938(4) |

Bond types: *C16-H16···O2/*$C_{ar}$–H···*O2*$_{diox}$, *C18-H18···O3/*$C_{ar}$–H···*ONO* and *C18-H18...N2/*$C_{ar}$–H...$N_{cyano}$, C15-H15···O1 and C19-H19···O1$^{ii}$ are intramolecular interactions, $C_{ar}$ is aromatic carbon atom, $O_{diox}$ is a dioxolene oxygen atom and $N_{cyano}$ is the nitrogen atom from the cyano group. Distances data from non-solvated crystals ***1*** and ***2*** were taken from references 19 and 20 respectively. Symmetry operations: *i*=x-1,y,z; *ii*=-x+1,-y+1,-z+1; *iii*= 1-x, -y, -z+1; ;*iv*= x+1,y,z; *v*=x,1+y, z; *vi*=x, y, z-1; *vii*=x, -y+1/2, z+1/2; *viii*=-x, -y+1, -z+1; *ix*= x, -y+1/2, z-1/2, x=-*x*+2, -*y*+1,-*z*+1, xi=x,y,z+1, xii=-x,1/2+y,1/2-z; xiii = x, -1/2-y,z; xiv = -x, -y, -z. * The labeling scheme was adapted to keep relation with the solvated structures.

## VTI properties

According to the variable temperature magnetic susceptibility data, ***1*** presents a non-cooperative whereas ***2*** presents a cooperative *hs*-[$Co^{+2}(SQ^{\bullet-})_2$]↔*ls*-[$Co^{+3}(SQ^{\bullet-})(Cat^{2-})$] transition.[19] VTI in ***1BZ***, ***1TL***, ***2TL*** and ***2BZ*** solvate samples were characterized by following the crystallographic parameters and in particular the *Co–L* distance changes in the *Co* first coordination shell. The interatomic distances obtained from the X-ray diffraction data provided two values for *Co–O* and one value for *Co–N* distance in each temperature. Refined distances for *Co–L* in pure state *hs*-[$Co^{+2}(SQ^{\bullet-})_2$] and *ls*-[$Co^{+3}(SQ^{\bullet-})(Cat^{2-})$] are in agreement with the values obtained from a survey of about 34 similar structures deposited in CCDC[28] (Table 2). Using the refined *Co–L* distances for a given temperature ($D_{exp}^{Co-L}$), we could compute the $Co^{2+}$ concentration for a given distance $[hs-Co^{2+}]_L$ by the following equation:

$$[hs-Co^{2+}]_L = \left(D_{exp}^{Co-L} - D_{Co^{3+}}^{Co-L}\right)/\left(D_{Co^{2+}}^{Co-L} - D_{Co^{3+}}^{Co-L}\right) \qquad (1)$$

Where *L* stands for *O* and *N* atoms, $D_{Co^{3+}}^{Co-L}$ and $D_{Co^{2+}}^{Co-L}$ are the values of *Co–L* distances in *ls*-[$Co^{+3}(SQ^{\bullet-})(Cat^{2-})$] and *hs*-[$Co^{+2}(SQ^{\bullet-})_2$] states, respectively. The average concentration $[hs-Co^{2+}]$ value for a given temperature was obtained averaging the values obtained for each Co ion neighbor. Thus,

$$[hs-Co^{2+}] = \sum_L [hs-Co^{2+}]_L \qquad L = O, N \qquad (2)$$

**Table 2*: Co-O* and *Co-N* interatomic distances.**

| *ls*-[$Co^{+3}(SQ^{\bullet-})(Cat^{2-})$] state | | *hs*-[$Co^{+2}(SQ^{\bullet-})_2$] state | |
|---|---|---|---|
| Refinement distances | | | |
| $Co^{3+}$-O | 1.886(4) Å | $Co^{2+}$-O | 2.052(8) Å |
| $Co^{3+}$-N | 1.958(3) Å | $Co^{2+}$-N | 2.184(6) Å |
| CCDC survey distances | | | |
| $Co^{3+}$-O | 1.86(1) Å | $Co^{2+}$-O | 2.04(2) Å |
| $Co^{3+}$-N | 1.94(1) Å | $Co^{2+}$-N | 2.17(3) Å |

analysis of the $[hs-Co^{2+}]$ shown in Figure 7 establishes that the *hs*-[$Co^{+2}(SQ^{\bullet-})_2$]↔*ls*-[$Co^{+3}(SQ^{\bullet-})(Cat^{2-})$] VTI in ***1TL***, ***2TL*** and ***2BZ*** is non-cooperative, occurring gradually in a temperature range between 250 K and 180 K. For all these tautomers, pure *ls*-[$Co^{+3}(SQ^{\bullet-})(Cat^{2-})$] states can only be achieved at temperatures below 150 K. ***1BZ*** crystals present a cooperative/abrupt VTI with hysteresis of ~30 K in which *ls*-[$Co^{+3}(SQ^{\bullet-})(Cat^{2-})$] pure state is observed below 120 K for cooling and up to 150 K during the heating processes.

During the VTI in all solvate tautomers, the intramolecular hydrogen bonds distances ($C_{ar}$–$H\cdots O_{diox}$) change dramatically to accommodate the changes in the local *Co* ion coordination while intermolecular hydrogen-bonded lattice ($C_{ar}$–$H\cdots O_{diox}$, $C_{ar}$–$H\cdots ONO$, $C_{ar}$–$H\cdots N_{cyano}$) change very little (Table 1). As a consequence, part of the structure must rotate, as evidenced by the change in the relative normal vector planes of the $NO_2$ in ***1BZ*** and ***1TL***, the ordering of the *t*-butyl groups and by the reorientation of the toluene/benzene solvate molecules in ***2BZ*** and ***2TL*** crystals. This is noted in Figure 2 in which the gradual accommodation of structure is confirmed by the smooth change in the angles formed by the solvent and pyridine ring planes. In the opposite way, for the sample with cooperative VTI, ***1BZ***, the angles formed by solvent and pyridine rings change abruptly. This evidences that the crystal packing hold the abrupt/smooth VTI character observed in the variation of bond length between metal and ligands.

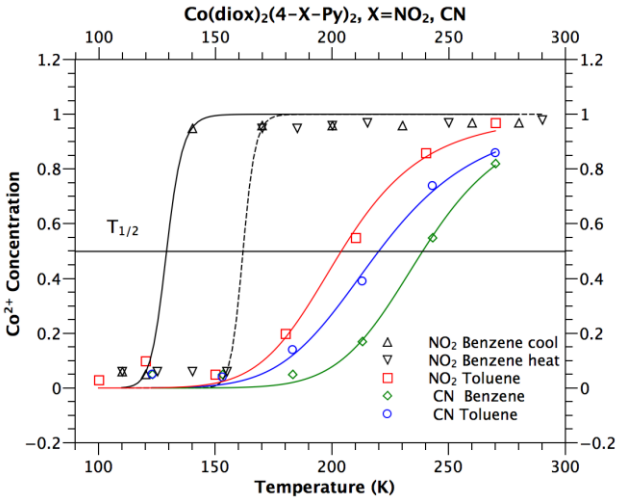


Figure 7: [*hs*–$Co^{2+}$] concentration during the interconversion *hs*-[$Co^{+2}(SQ^{\bullet-})_2$]↔*ls*-[$Co^{+3}(SQ^{\bullet-})(Cat^{2-})$]. The fittings were performed by least square procedures according with the equilibrium equation (4). $T_{1/2}$ is the temperature in which [*hs*–$Co^{2+}$]=[*ls*-$Co^{3+}$]

As already highlighted in Figure 3 and in Figure 6, all the solvate tautomers present distances between interacting layers of [Co*(diox)*$_2$(4-X-py)$_2$] X=$NO_2$,CN molecules of ~15 Å, whereas in the non-solvate ones these distances are ~11.6 Å. Since ***1BZ*** and ***2*** crystals present a cooperative VTI, the layer separation alone does not explain the lack of cooperativity in ***1TL***, ***2TL*** and ***2BZ***. Indeed, ***1TL***, ***2TL*** and ***2BZ*** crystals have the same crystal packing and similar intermolecular interactions as their non-solvate ***1*** and ***2*** relatives, whereas ***1BZ*** present a unique intermolecular network. Therefore, the number and the strength of the intermolecular interactions might also play an important role in the cooperativity. Remarkably, each [Co(diox)$_2$(4-$NO_2$-py)$_2$] molecule in the ***1BZ*** crystal make eight hydrogen bonds with their neighbors, being four of them of the type $C_{ar}$–$H\cdots O_{diox}$ involving oxygen atoms directly bounded to the *Co* ions. Thus the *Co* atom coordination shell expansion/contraction during the *hs*-[$Co^{+2}(SQ^{\bullet-})_2$]↔*ls*-[$Co^{+3}(SQ^{\bullet-})(Cat^{2-})$] interconversion could be readily transmitted trough neighbor molecules contributing for the cooperativity. It is worth noting that ***1BZ*** crystal present the shortest $C_{ar}$–$H\cdots O_{diox}$ hydrogen contact distances and consequently the shortest in layer *Co-Co* separation, among all investigate solvate crystals (Table 1).

## VTI Thermodynamics

Thermodynamic parameters of the tautomeric *hs*-[$Co^{+2}(SQ^{\bullet-})_2$]↔*ls*-[$Co^{+3}(SQ^{\bullet-})(Cat^{2-})$] interconversion can be

obtained from the fitting of the $[hs-\mathrm{Co}^{2+}]$ data shown in (Figure 7), using the equilibrium equation below:

$$K_{VT} = \frac{[hs-\mathrm{Co}^{3+}]}{[ls-\mathrm{Co}^{2+}]} = exp\left(-\frac{\Delta G}{RT}\right). \quad (3)$$

Since $\left[ls-\mathrm{Co}^{3+}\right] = (1 - [hs-\mathrm{Co}^{2+}])$ and $\Delta G = \Delta H - T\Delta S$,

$$[hs-\mathrm{Co}^{2+}] = 1/[exp\left(\frac{\Delta H}{RT} - \frac{\Delta S}{R}\right) + 1] \quad (4)$$

where $\Delta G$ is the Gibbs energy change, $\Delta H$ is the enthalpy change, $\Delta S$ is the entropy change, T is Temperature and $R$ = 8.314 J/Kmol. The values of $\Delta H$ and $\Delta S$ listed in Table 3 were obtained from the least-square fit of [*hs*–$Co^{2+}$] data shown in Figure 7. $T_{1/2}$ (the temperature in which [*hs*–$Co^{2+}$]=[*ls*-$Co^{3+}$]) was obtained from the interception between fitted curves and the horizontal line drawn in Figure 7. With the exception of the $\Delta S$ value of the ***1BZ***, all the remaining values obtained are similar to the ones found in related complexes.[2930].

**Table 3 Enthalpy ($\Delta H$) and entropy ($\Delta S$) change during the *hs*-[$Co^{+2}(SQ^{\bullet-})_2$] ↔*ls*-[$Co^{+3}(SQ^{\bullet-})(Cat^{2-})$] interconversion.**

| | $T_{1/2}$ (K) | ΔH (kJ/mol) | ΔS (J/K) |
|---|---|---|---|
| ***1BZ*** Cooling | 145 | 136(8) | 938(57) |
| ***1BZ*** Heating | 165 | 198(2) | 1198(13) |
| ***1TL*** | 207 | 23(2) | 110(11) |
| ***2TL*** | 222 | 22(1) | 99(5) |
| ***2BZ*** | 241 | 30(2) | 126(6) |

## Conclusion

The structure of the solvate ***1BZ*** crystal is described by the triclinic $P\bar{1}$ space group symmetry with Z=1. ***1TL***, ***2TL*** and ***2BZ*** solvate crystal structures are described by the $P2_1/c$ symmetry with Z=2. ***1TL***, ***2BZ*** and ***2TL*** show a non-cooperative VTI occurring gradually in a temperature range between 250 K and 180 K. For all these crystals, pure *ls*-[$Co^{+3}(SQ^{\bullet-})(Cat^{2-})$] states can only be achieved at temperatures below 150 K. ***1BZ*** crystals present a cooperative interconversion with hysteresis of ~30 K in which *ls*-[$Co^{+3}(SQ^{\bullet-})(Cat^{2-})$] pure state is observed below 120 K for cooling and up to 150 K during the heating processes. VTI in all these crystals are characterized by an isotropic change in the *Co–N* and *Co–O* distances, an anisotropic change in the unit cell volume, the reorientation of the solvents molecules and pyridine ring planes and by a invariance in the intermolecular hydrogen-bonded lattice. Due to the steric hindrance of the *t*-butyl only one oxygen atom of the dioxolene group coordinating the metal ion is involved in intermolecular interactions with $C_{ar}$–*H* groups. Together all these structure accommodation effects and in particular the strength and the number of direct contacts towards the dioxolene oxygen atoms, seem to account for the VTI properties.

All the solvate tautomers present distances between interacting layers of [Co*(diox)*$_2$(4-X-py)$_2$] X=$NO_2$,CN molecules of ~15 Å, whereas in the non-solvate ones these distances are ~11.6 Å. Remarkably, when compared with ***1TL***, ***2BZ*** and ***2TL*** crystals as well as with the non solvated ***1*** and ***2*** crystals, ***1BZ*** present the shortest and therefore the strongest $C_{ar}$–$H^{\cdots}O_{diox}$ hydrogen as well as the shortest *Co–Co* distances. Cooperativity in the VTI of ***1BZ,*** in contrast to ***2*** that also presents cooperative VTI, seems to be related with the number and particularly with the strength of the $C_{ar}$–$H^{\cdots}O_{diox}$ interaction and with its correspondent *Co–Co* separation. Thus benzene and toluene solvation of ***1*** and ***2*** crystals plays a key role in the definition of the nature of the VTI observed in these compounds, despite the solvates molecules are not directly involved in the intermolecular contact network of the [Co*(diox)*$_2$(4-X-py)$_2$] X=$NO_2$,CN molecules.

## ASSOCIATED CONTENT

Crystallographic data (CIF) and pictures about intramolecular and intermolecular interactions**.** "This material is available free of charge via the Internet at http://pubs.acs.org

## AUTHOR INFORMATION

### Corresponding Author

* Carlos Basílio Pinheiro. Departamento de Física – Universidade Federal de Minas Gerais. Av. Antônio Carlos 6627.Cx 702. CEP 31270-901. Belo Horizonte, MG – Brazil. Tel +55-31-3409-6600. *E-mail: cbpinheiro@ufmg.br

### Author Contributions

The manuscript was written through contributions of all authors. All authors have given approval to the final version of the manuscript.

## ACKNOWLEDGMENT

Will Gee for helping with crystal growth at controlled atmosphere at University of Bath. PRR is grateful to the Engineering and Physical Sciences Research Council (EPSRC) UK for funding (EP/K004956 & EP/G067759)for the project. CBP thanks FAPEMIG (APQ-00388-13), CNPq (308354/2012-5; 448723/2014-0) and CAPES (10030-12-3) for financial support. We also thank CNPq for the PhD fellowship of MAR.

## ABBREVIATIONS

VTI – Valence Tautomerism Interconversion. ***1BZ***=[Co*(diox)*$_2$(4-$NO_2$-py)$_2$]·benzene, ***1TL***=[Co*(diox)*$_2$(4-$NO_2$-py)$_2$]·toluene, ***2BZ***= [Co*(diox)*$_2$(4-CN-py)$_2$]·benzene and ***2TL***=[Co*(diox)*$_2$(4-CN-py)$_2$]·toluene crystals

## REFERENCES

1 O. Kahn, *Science*, 1998, **279**, 44.

[2]B.L.Feringa,MolecularSwitches,Wiley-VCH,Weinheim,2001.

[3]Gütlich, P. and Dei, A. *Angew.Chem. Int. Ed. Engl.* 1997, ***37***, 2734.

[4]Novio, F.; Evangelio, E.; Vazquez-Mera, N.; González-Monje, P.; Bellido, E.; Mendes, S.; Kehagias, N. Ruiz-Molina, D., *ScientificReports*, 2013, **3,**1-7,.

[5] D. A. Shultz (2002). Valence Tautomerism in Dioxolene Complexes of Cobalt. In In*Magnetism: Molecules to Materials II: Molecule-Based Materials*. Edited by Joel S. Miller and Marc Drillon. *Wiley-VchVerlagGmbh& Co. KGaA*.

[6]Sato, O.; Hayami, S.; Gu, Z.-Z.; Seki, K.; Nakjima, R.; Fujishima, A.; *Chem. Lett.***2001,** 874

[7]Varret, F.; Nogues, M.; Goujon, A. In *Magnetism: Molecules to Materials;* Miller, J. S.; Drillon, M.; eds., Wiley-VCH: Weinheim, 2001

[8]Poneti, G., Mannini, M., Sorace, L., Sainctavit, P., Arrio, M. A., Otero, E., Cezar, J. C.,Dei, A. (2010). *Angew. ChemieInt. Ed*, **49**, 1954.

[9] T. M. Francisco, D. A. Shultz, P. Raithby and C. B. Pinheiro (2015). *To be published*.

[10] D. N. Hendrickson and C. G. Pierpont (2004). *Top. Curr. Chem*., **234**, 63

[11] A. Dei, D. Gatteschi, C. Sangregorio and L. Sorace (2004). *Acc. Chem. Res*., **37**, 827-835.

[12] S. Decurtins, P. Gutlich, K. M. Hasselbach, A. Hauser and H. Spiering, *Inorganic Chemistry*, 1985, **24**, 2174-2178.

[13] Sato, O.; Hayami, S.; Gu, Z.-Z.; Seki, K.; Nakjima, R.; Fujishima, A.; *Chem. Lett.***2001,** 874

[14]Varret, F.; Nogues, M.; Goujon, A. In *Magnetism: Molecules to Materials;* Miller, J. S.; Drillon, M.; eds., Wiley-VCH: Weinheim, 2001

[15]Carbonera, C.; Dei, A.; Létard, J.-F.; Sangregorio, C.; Sorace, L. *Inorg. Chim. Acta* **2007**, *360* (13), 3825–3828

[16]Beni, A.; Dei, A.; Laschi, S.; Rizzitano, M.; Sorace, L. *Chem.sEur. J.* **2008**, *14* (6), 1804–1813

[17] C. G. Pierpont (2001). *Coord. Chem. Rev*, **216–217**, 99–125

[18] Adams, D. M., Dei, A., Rheingold, A. L., Hendrickson, D. N..*Angew. Chemie, Int. Ed. Engl*. **1993**, 32, 880.

[19] R. D. Schmidt, D. A. Shultz, J. D. Martin and P. D. Boyle (2010). *J. Am. Chem. Soc*., **132**, 6261-627.

[20] Robert D. Schmidt, David A. Shultz and James D. Martin (2010). Inorg. Chem., ***49***, 3162–3168

[21]Agilent Technologies (2011). Agilent Technologies UK Ltd., Oxford, UK, Xcalibur CCD system, CrysAlisPro Software system, Version 1.171.35.21.

[22]Analytical numeric absorption correction using a multifaceted crystal model based on expressions derived by R. C. Clark and J. S. Reid. (R. C. Clark and J. S. Reid, *ActaCryst. A*, 1995, **51**, 887).

[23]Empirical absorption correction using spherical harmonics, implemented in SCALE3 ABSPACK scaling algorithm.

[24]G. M. Sheldrick, *ActaCryst. A*, 2008, **64**, 112.

[25]Altomare, A., Cascarano, G., Giacovazzo, C., Guagliardi, A., Burla, M. C., Polidori, G. &Camalli, M. (1994). J. Appl. Cryst.27, 435.

[26]G. M. Sheldrick, *ActaCryst. A*,2008, **64**, 112.

[27]C. K. Johnson, in *Crystallographic Computing*, ed. F. R. Ahmed, Munksgaard, Copenhagen, 1970, p. 207 – 219

[28] F. H. Allen, *Acta Cryst*.,**B58**, 380-388, 2002

[29] (a) Adams, D. M., Hendrickson, D. N. *J. Am. Chem. Soc*.1996, *118*, 11515. (b) Sofi Bin-Salamon , Scott H. Brewer, Ezra C. Depperman, Stefan Franzen, Jeff W. Kampf, Martin L. Kirk, R. Krishna Kumar, Simon Lappi, Katrina Peariso, Kathryn E. Preuss, and David A. Shultz. *Inorganic Chemistry*, 2006,***45***, 4461-4467

[30] Pierpont, C. G., Jung, O. -S. *Inorg. Chem.* 1995, ***34***, 4281.